Structural Basis for Inhibitor Specificity in Human Poly(ADP-ribose) Polymerase-3†

Lari Lehtiö,[‡,§] Ann-Sofie Jemth,[||] Ruairi Collins,[‡] Olga Loseva,[||] Andreas Johansson,[‡] Natalia Markova,[‡,⊥] Martin Hammarström,[‡] Alex Flores,[‡] Lovisa Holmberg-Schiavone,[‡,§] Johan Weigelt,[‡] Thomas Helleday,*[,||,#] Herwig Schüler,*[,‡] and Tobias Karlberg[‡]

Structural Genomics Consortium, Department of Medical Biochemistry and Biophysics, Karolinska Institutet, SE-17177 Stockholm, Sweden. Department of Genetics, Microbiology, and Toxicology, Stockholm University, SE-10691 Stockholm, Sweden. iNovacia AB, SE-11251 Stockholm, Sweden. Gray Institute for Radiation Oncology & Biology, University of Oxford, Oxford OX3 7DQ, United Kingdom

Received January 15, 2009

Poly(ADP-ribose) polymerases (PARPs) activate DNA repair mechanisms upon stress- and cytotoxin-induced DNA damage, and inhibition of PARP activity is a lead in cancer drug therapy. We present a structural and functional analysis of the PARP domain of human PARP-3 in complex with several inhibitors. Of these, KU0058948 is the strongest inhibitor of PARP-3 activity. The presented crystal structures highlight key features for potent inhibitor binding and suggest routes for creating isoenzyme-specific PARP inhibitors.

Downloaded by Jonathan Berry on September 11, 2009 | http://pubs.acs.org
Publication Date (Web): April 8, 2009 | doi: 10.1021/jm900052j

Introduction

PolyADP ribosylation is a ubiquitous protein modification involved in the regulation of transcription, cell proliferation, differentiation, and apoptosis.[1,2] Of the 17 human poly(ADP ribose) polymerase (PARP)[a] enzymes, at least PARP-1, PARP-2 and tankyrase-1 (PARP-5a) are required for the maintenance of genome stability.[3] PARP-1 has important roles in DNA single-strand break and base excision repair.[4] Inhibition of PARP-1 activity may have beneficial effects in a variety of diseases, including stroke, myocardial infarction, heart failure, and diabetes mellitus, where extensive DNA damage may lead to fatigue and tissue necrosis.[5] PARP inhibitors also efficiently and selectively kill BRCA2 defective tumors in monotherapy.[6,7] While PARP inhibitors are in numerous clinical trials,[8] it is unclear whether they act on PARP-1 alone or also on other PARP family members. Given the high degree of conservation of the active sites among these proteins, off-target effects may be expected. Therefore, to better understand the effects of PARP inhibition in disease treatment, information on the specificity and selectivity of PARP inhibitors is urgently needed.

Results and Discussion

PARP-3 is a poorly characterized family member with extensive homology to PARP-1 and -2. We determined the crystal structure of the PARP domain (residues 178−532) of human PARP-3. Details of the structure determination and refinement are summarized in Table S1 in the Supporting Information. The PARP-3 structure consists of an N-terminal α-helical domain and a C-terminal α/β-domain (Figure 1). As expected based on sequence similarity (~35% identity between the PARP domains), this structure is similar to the previously reported structures of the PARP-1 and PARP-2 PARP domains.[9−11] The C-terminal domain contains the PARP signature motif (β-α-loop-β-α) on its inner surface, forming the NAD^+ donor binding crevice located between the two domains. The C-terminal domain is also similar to that of PARP-5a/tankyrase-1.[12] The residues lining the active site are largely conserved between PARP-1 and -3, apart from a few notable exceptions.

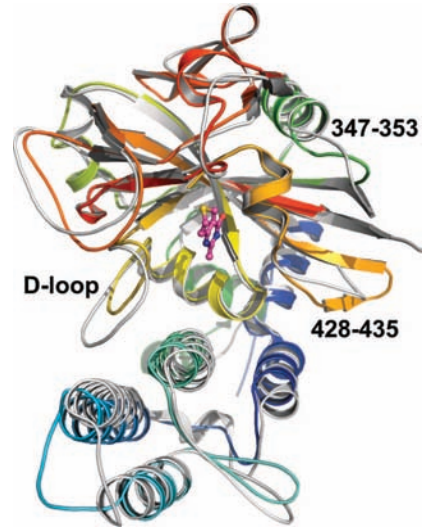

Figure 1. Comparison of PARP-3 and PARP-1 structures. Overall comparison of the catalytic fragments of PARP-3 (PDB entry 3C4H) and PARP-1 (PDB entry 2RD6). Blue to red, PARP-3; gray, PARP-1. Ligand **2** from structure 3C4H is shown as a ball-and-stick model to indicate the position of the active site between the domains. Loops surrounding the acceptor site that differ the most between PARP-1 and PARP-3 are labeled, as well as the D-loop lining the NAD^+ binding site. The D-loop in PARP-3 (residues 398−411) adopts a different conformation, which affects packing of the long helix (residues 233−241) in the N-terminal domain. In addition the D-loop is four residues shorter in PARP-3. These differences in the D-loops may affect the binding affinities of the known PARP inhibitors. PARP-3 structure 3C4H superposes with an rmsd of 1.4 Å to human PARP-1 (2RD6; 319 Cα atoms).

The most important differences between the PARP-3 and PARP-1 PARP domains lie in the loops surrounding the active site. The donor site loop (D-loop) in PARP-3 (residues

† PDB IDs for the PARP-3 inhibitor complexes: 3FHB, 3C4H, 3C49, and 3CE0.

* To whom correspondence should be addressed. For T.H.: phone, +468162914; fax, +468164315; E-mail, helleday@gmt.su.se. For H.S.: phone, +46852486843; fax, +46852486868; E-mail, herwig.schuler@mbb.ki.se.

‡ Structural Genomics Consortium, Karolinska Institutet.

§ Present address: For L.L.: Department of Biochemistry and Pharmacy, Åbo Akademi, FI-20520 Turku, Finland. For L.H.S.: Structural Chemistry Laboratory, AstraZeneca R&D, SE-43150 Mölndal, Sweden.

|| Department of Genetics, Microbiology and Toxicology, Stockholm University.

⊥ iNovacia AB.

Gray Institute for Radiation Oncology & Biology, University of Oxford.

[a] Abbreviations: ITC, isothermal titration calorimetry; NAD^+, nicotinamide adenine dinucleotide; PARP, poly(ADP ribose) polymerase.

10.1021/jm900052j CCC: $40.75 © 2009 American Chemical Society
Published on Web 04/08/2009

Table 1. Summary of PARP-3 Inhibitor Complexes Used in This Study

PARP-3						PARP-1	
Compound	**Structure**	**PDB id.**	**T_m (°C)** [a]	**ΔT_m (K)**	**K_d (μM)** [b]	**K_d (μM)** [b]	**Lit. IC_{50} or K_d (μM)** [c]
-		-	48 ± 0.5 [d]				
1	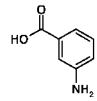	3FHB	54	6	>2	n.d.	-
2	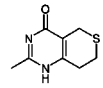	3C4H	54	6	2 ± 0.2	0.15 ± 0.065	0.2
3	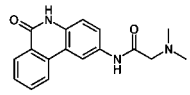	3CE0	54	6	0.7 ± 0.15	0.11 ± 0.064	0.11
4	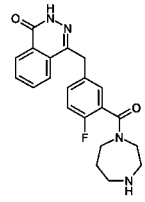	3C49	62	14	0.07 ± 0.008	0.019 ± 0.0055	0.0034

[a] Transition midpoints in thermal denaturation experiments. [b] Apparent K_d values as determined by isothermal titration calorimetry. For comparison, apparent affinities for PARP-$1^{654-1013}$ were also determined. [c] Previously published estimates for either K_d (compound **2**, ref 16) or IC_{50} values (compound **3**, ref 17, and compound **4**, ref 18). [d] Transition midpoint for PARP-$3^{178-532}$ alone (control).

Downloaded by Jonathan Berry on September 11, 2009 | http://pubs.acs.org
Publication Date (Web): April 8, 2009 | doi: 10.1021/jm900052j

398−411) is four residues shorter than in PARP-1, which results in a slightly opened pocket between the donor site and the N-terminal α-helix bundle (Figure 1). Further differences between PARP-3 and PARP-1 are in a loop (residues 347−353) near the acceptor site and a loop (residues 428−435) following the PARP-signature motif (Figure 1). The crystal structure of PARP-3 is described in further detail in the Supporting Information.

We initially solved the structure of PARP-3 in complex with the inhibitor analogue **1** (3ABA). To further explore potential inhibitor interactions we assembled a small library of PARP-1 inhibitors based on the literature[13,14] and evaluated their effect on PARP-$3^{178-532}$ using a thermal stabilization assay.[15] This screen revealed three compounds that significantly raised the midpoints of the thermal transitions, namely **2** (DR2313),[16] **3** (PJ34),[17] and **4** (KU0058948).[18] The largest change was observed with **4**, which gave a shift of 14 K (Table 1). Isothermal titration calorimetry (ITC) established the apparent affinities of PARP-3 for these compounds and confirmed that **4** bound tighter to PARP-3 than did the other compounds (Table 1). Control experiments using the PARP domain of human PARP-1 suggested that **4** bound about 3-fold tighter to PARP-1 than to PARP-3. The values we determined for PARP-1 compare favorably with literature values (Table 1).

We investigated the ADP ribosylation activity of full-length human PARP-3. In the presence of biotinylated NAD^+, the protein was capable of auto-ADP ribosylation (Figure 2) as well as ADP ribosylation of histone H1, a previously unknown substrate for PARP-3 (data not shown). Activity measurements in the presence of the above PARP inhibitors established the active concentration ranges for these compounds (Figure 2), and these were in agreement with the binding constants determined by ITC (Table 1). Compound **4** was the most potent inhibitor of PARP-3 activity (Figure 2a and Supporting Information, Figure S1), but **4** inhibited PARP-1 more potently than PARP-3 (Figure 2b), as expected from the apparent affinities determined by ITC.

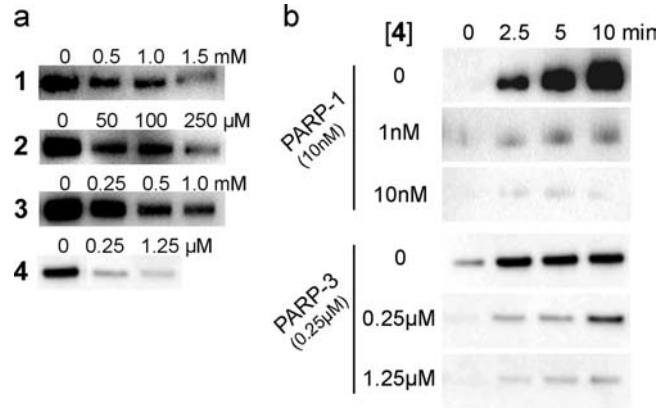

Figure 2. Effect of canonical PARP inhibitors on the catalytic activity of PARP-3. (a) Inhibition of PARP-3 auto-ADP ribosylation with different inhibitors (bold numbers; see main text for identification). Full length recombinant PARP-3 (250 nM) was automodified using 25 μM of biotinylated NAD^+ as substrate. Note that compound **4** is the most potent PARP-3 inhibitor. (b) Comparison of the dose-dependent inactivation of PARP-1 and PARP-3 by compound **4**. Full length recombinant PARP-1 and PARP-3 were automodified in the presence of the indicated concentrations of the inhibitor. Automodified PARP-1 (upper panel) and PARP-3 (lower panel) were visualized by Western blotting using an antibiotin antibody. Details of the assay conditions are given in the Supporting Information.

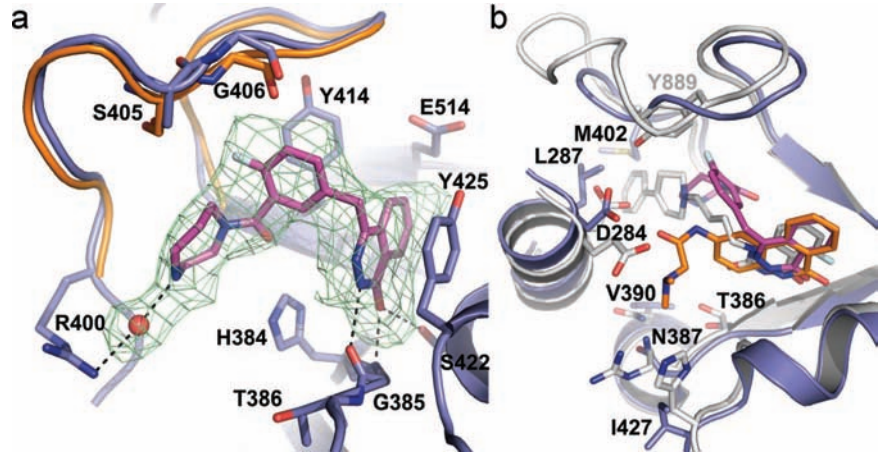

Figure 3. Crystal structures of canonical PARP inhibitors in complex with PARP-3. (a) Interactions of PARP-3 with **4**, with an omit map rendered at 2σ. Orange, D-loop of the complex with the smaller compound **2** (PDB entry 3C4H) shown to illustrate the displacement of Gly406 by 1 Å and the tighter arrangement of the D-loop upon binding of **4**. The central fluorobenzyl ring of **4** forms $\pi-\pi$ stacking with the Tyr414 side chain, and the carbonyl between the fluorobenzyl and diazepam rings forms a hydrogen bond with the backbone amine of Tyr414. Further, the diazepam ring makes hydrophobic interactions with Arg400 and Ile413 and **4** interacts with Arg400 via a water molecule at the bottom of the NAD^+ binding cleft. Notably, Glu514 is not conserved in the PARP family and could be used for enhancing selectivity in drug design. (b) Superposition of the donor sites. Blue, PARP-3; gray, PARP-1 (1UK1). Inhibitors **3** (orange) and **4** (magenta) bound to PARP- 3 are compared with **5** (gray) bound to PARP-1. Nonconserved residues between PARP-3 and PARP-1 are labeled to indicate the different environments of **3** and **4** in the binding sites that could be utilized in the design of more selective inhibitors. Compound **5** is predicted to clash with Met402 of PARP-3.

Downloaded by Jonathan Berry on September 11, 2009 | http://pubs.acs.org
Publication Date (Web): April 8, 2009 | doi: 10.1021/jm900052j

We solved crystal structures of PARP-$3^{178-532}$ inhibitor complexes with **1**, **2**, **3**, and **4** at 2.1−2.8 Å resolution (Figure 3, Table 1, Supporting Information, Table S1, and Supporting Information, Figure S2). In all four structures, the inhibitors stack against the Tyr425 and Tyr414 side chains (Figure 3a and Supporting Information, Figure S2). All compounds also form hydrophobic interactions with the catalytic Glu514. In strong contrast with the other complexes, the PARP-3 complex with compound **4** features a number of key interactions between protein and inhibitor that may explain its high affinity and potent inhibitory and thermostabilizing effect (Figure 3a and Supporting Information, Figure S2).

Although the nicotinamide binding pockets of PARP-3 and PARP-1 are highly conserved, there are differences at the site where known PARP inhibitors interact (Figure 3b). Notably the D-loop (substitution Met402Ala between PARP-3 and PARP-1, and PARP-1 specific Tyr889), the long helix of the C-terminal lobe (Asp284Glu and Leu287Asp), and the N-terminal side of the donor site (Thr386Ser, Asn387Arg, Val390Asn, and Ile427His) all contain sequence differences between PARPs that may be exploited for rational design of isoenzyme specific inhibitors. This is best illustrated by interaction of **4** with the D-loop of PARP-3, resulting in structural changes in the D-loop and tighter binding. Compounds extending to the binding site of the NAD^+ adenosine moiety may clash with the PARP-3 D-loop similarly as **5** (FR257517)[19] appears to clash with Met402 (Figure 3b). Smaller inhibitors that mainly interact with the nicotinamide binding pocket will likely bind to different PARPs with similar affinity; on the other hand, inhibitors interacting with the opposite end of the binding site are more likely to contribute to selectivity among isoenzymes, as we show for **3** (Table 1). Selectivity between PARPs might be achieved by introducing novel contacts, or clashes, between inhibitor compounds and the carboxyl group of Glu514 because many of the PARPs lack glutamic acid in this position (Figure 3a).

Conclusion

In conclusion, while the structures of the PARP domains of PARP-3 and PARP-1 are overall similar and the nicotinamide binding clefts are conserved, they differ in the length and position of their D-loops and the lower surfaces of their donor sites constitute different environments. Our crystal structures of PARP-3 in complex with one potent and three weaker inhibitors revealed structural features that will be useful in the rational design of selective PARP inhibitors.

Acknowledgment. We thank Dr. Graeme Smith for materials, Susanne van den Berg for technical assistance, and The Swedish Cancer Society (T.H.), the Swedish Children's Cancer Foundation (T.H.), the Swedish Research Council (T.H.), the Swedish Pain Relief Foundation (T.H.), and the Medical Research Council (T.H.) for supporting this work financially. The Structural Genomics Consortium is a registered charity (no. 1097737) that receives funds from the Canadian Institutes for Health Research, the Canadian Foundation for Innovation, Genome Canada through the Ontario Genomics Institute, GlaxoSmithKline, Karolinska Institutet, the Knut and Alice Wallenberg Foundation, the Ontario Innovation Trust, the Ontario Ministry for Research and Innovation, Merck & Co., Inc., the Novartis Research Foundation, the Swedish Agency for Innovation Systems, the Swedish Foundation for Strategic Research, and the Wellcome Trust. We gratefully acknowledge the support by personnel at the ESRF synchrotron radiation facility.

Supporting Information Available: Further description of the PARP-3 crystal structures; table summarizing data collection and refinement statistics; figure demonstrating inhibitor effects on PARP-3 enzymatic activity; figure summarizing ligand interactions with PARP-3; materials and methods section. This material is available free of charge via the Internet at http://pubs.acs.org.

References

(1) Bürkle, A. Poly(ADP-ribose). The most elaborate metabolite of NAD^+. *FEBS J.* **2005**, *272*, 4576–4589.

(2) Schreiber, V.; Dantzer, F.; Ame, J. C.; de Murcia, G. Poly(ADP-ribose): novel functions for an old molecule. *Nat. Rev. Mol. Cell Biol.* **2006**, *7*, 517–528.

(3) Ménissier de Murcia, J.; Ricoul, M.; Tartier, L.; Niedergang, C.; Huber, A.; Dantzer, F.; Schreiber, V.; Amé, J. C.; Dierich, A.; LeMeur, M.;

Sabatier, L.; Chambon, P.; de Murcia, G. Functional interaction between PARP-1 and PARP-2 in chromosome stability and embryonic development in mouse. *EMBO J.* **2003**, *22*, 2255–2263.
(4) Satoh, M. S.; Lindahl, T. Role of poly(ADP-ribose) formation in DNA repair. *Nature (London)* **1992**, *356*, 356–358.
(5) Pacher, P.; Szabo, C. Role of poly(ADP-ribose) polymerase 1 (PARP-1) in cardiovascular diseases: the therapeutic potential of PARP inhibitors. *Cardiovasc. Drug Rev.* **2007**, *25*, 235–260.
(6) Bryant, H. E.; Schultz, N.; Thomas, H. D.; Parker, K. M.; Flower, D.; Lopez, E.; Kyle, S.; Meuth, M.; Curtin, N. J.; Helleday, T. Specific killing of BRCA2-deficient tumours with inhibitors of poly(ADP-ribose) polymerase. *Nature (London)* **2005**, *434*, 913–917.
(7) Farmer, H.; McCabe, N.; Lord, C. J.; Tutt, A. N.; Johnson, D. A.; Richardson, T. B.; Santarosa, M.; Dillon, K. J.; Hickson, I.; Knights, C.; Martin, N. M.; Jackson, S. P.; Smith, G. C.; Ashworth, A. Targeting the DNA repair defect in BRCA mutant cells as a therapeutic strategy. *Nature (London)* **2005**, *434*, 917–921.
(8) Helleday, T.; Petermann, E.; Lundin, C.; Hodgson, B.; Sharma, R. A. DNA repair pathways as targets for cancer therapy. *Nat. Rev. Cancer* **2008**, *8*, 193–204.
(9) Ruf, A.; Mennissier de Murcia, J.; de Murcia, G.; Schulz, G. E. Structure of the catalytic fragment of poly(AD-ribose) polymerase from chicken. *Proc. Natl. Acad. Sci. U.S.A.* **1996**, *93*, 7481–7485.
(10) Oliver, A. W.; Amé, J. C.; Roe, S. M.; Good, V.; de Murcia, G.; Pearl, L. H. Crystal structure of the catalytic fragment of murine poly(ADP-ribose) polymerase-2. *Nucleic Acids Res.* **2004**, *32*, 456–464.
(11) Kinoshita, T.; Nakanishi, I.; Warizaya, M.; Iwashita, A.; Kido, Y.; Hattori, K.; Fujii, T. Inhibitor-induced structural change of the active site of human poly(ADP-ribose) polymerase. *FEBS Lett.* **2004**, *556*, 43–46.
(12) Lehtiö, L.; Collins, R.; van den Berg, S.; Johansson, A.; Dahlgren, L. G.; Hammarström, M.; Helleday, T.; Holmberg-Schiavone, L.; Karlberg, T.; Weigelt, J. Zinc binding catalytic domain of human tankyrase 1. *J. Mol. Biol.* **2008**, *379*, 136–145.
(13) Peukert, S.; Schwahn, U. New inhibitors of poly(ADP-ribose) polymerase (PARP). *Expert Opin. Ther. Pat.* **2004**, *14*, 1531–1551.
(14) Curtin, N. J. PARP inhibitors for cancer therapy. *Expert Rev. Mol. Med.* **2005**, *7*, 1–20.
(15) Niesen, F. H.; Berglund, H.; Vedadi, M. The use of differential scanning fluorimetry to detect ligand interactions that promote protein stability. *Nat. Protoc.* **2007**, *2*, 2212–2221.
(16) Nakajima, H.; Kakui, N.; Ohkuma, K.; Ishikawa, M.; Hasegawa, T. A newly synthesized poly(ADP-ribose) polymerase inhibitor, DR2313 [2-methyl-3,5,7,8-tetrahydrothiopyrano[4,3-*d*]-pyrimidine-4-one]: pharmacological profiles, neuroprotective effects, and therapeutic time window in cerebral ischemia in rats. *J. Pharmacol. Exp. Ther.* **2005**, *312*, 472–481.
(17) Jagtap, P.; Soriano, F. G.; Virág, L.; Liaudet, L.; Mabley, J.; Szabó, E.; Haskó, G.; Marton, A.; Lorigados, C. B.; Gallyas, F., Jr.; Sümegi, B.; Hoyt, D. G.; Baloglu, E.; VanDuzer, J.; Salzman, A. L.; Southan, G. J.; Szabó, C. Novel phenanthridinone inhibitors of poly (adenosine 5′-diphosphate-ribose) synthetase: potent cytoprotective and antishock agents. *Crit. Care Med.* **2002**, *30*, 1071–1082.
(18) McCabe, N.; Lord, C. J.; Tutt, A. N.; Martin, N. M.; Smith, G. C.; Ashworth, A. BRCA2-deficient CAPAN-1 cells are extremely sensitive to the inhibition of poly(ADP-ribose) polymerase: an issue of potency. *Cancer Biol. Ther.* **2005**, *4*, 934–936.
(19) Iwashita, A.; Tojo, N.; Matsuura, S.; Yamazaki, S.; Kamijo, K.; Ishida, J.; Yamamoto, H.; Hattori, K.; Matsuoka, N.; Mutoh, S. A novel and potent poly(ADP-ribose) polymerase-1 inhibitor, FR247304 (5-chloro-2-[3-(4-phenyl-3,6-dihydro-1(2*H*)-pyridinyl)propyl]-4(3*H*)-quina zolinone), attenuates neuronal damage in in vitro and in vivo models of cerebral ischemia. *J. Pharmacol. Exp. Ther.* **2004**, *310*, 425–436.

JM900052J

Downloaded by Jonathan Berry on September 11, 2009 | http://pubs.acs.org
Publication Date (Web): April 8, 2009 | doi: 10.1021/jm900052j